Low-power silicon-organic hybrid (SOH) modulators for advanced modulation formats

M. Lauermann,[1,*] R. Palmer,[1,5] S. Koeber,[1,2,6] P. C. Schindler,[1,7] D. Korn,[1] T. Wahlbrink,[3] J. Bolten,[3] M. Waldow,[3] D. L. Elder,[4] L. R. Dalton,[4] J. Leuthold,[1,8] W. Freude,[1,2] and C. Koos[1,2,9]

[1]*Institute of Photonics and Quantum Electronics, Karlsruhe Institute of Technology, 76131 Karlsruhe, Germany*
[2]*Institute of Microstructure Technology, Karlsruhe Institute of Technology, 76344 Eggenstein-Leopoldshafen, Germany*
[3]*AMO GmbH, 52074 Aachen, Germany*
[4]*University of Washington, Department of Chemistry, Seattle, WA 98195-1700, USA*
[5] *Now with: Coriant GmbH, Munich, Germany*
[6] *Now with: University of Cologne, Chemistry Department, 50939 Köln, Germany*
[7] *Now with: Infinera Corporation, Sunnyvale, CA, USA*
[8]*Now with: Institute of Electromagnetic Fields, Swiss Federal Institute of Technology (ETH), Zurich, Switzerland*
[9]*christian.koos@kit.edu*
**matthias.lauermann@kit.edu*

Abstract: We demonstrate silicon-organic hybrid (SOH) electro-optic modulators that enable quadrature phase-shift keying (QPSK) and 16-state quadrature amplitude modulation (16QAM) with high signal quality and record-low energy consumption. SOH integration combines highly efficient electro-optic organic materials with conventional silicon-on-insulator (SOI) slot waveguides, and allows to overcome the intrinsic limitations of silicon as an optical integration platform. We demonstrate QPSK and 16QAM signaling at symbol rates of 28 GBd with peak-to-peak drive voltages of 0.6 V_{pp}. For the 16QAM experiment at 112 Gbit/s, we measure a bit error ratio of 5.1×10^{-5} and a record-low energy consumption of only 19 fJ/bit.

OCIS codes: (250.7360) Waveguide modulators; (060.4080) Modulation; (230.7370) Waveguides; (250.5300) Photonic integrated circuits.

References and links

1. K. Goi, A. Oka, H. Kusaka, Y. Terada, K. Ogawa, T.-Y. Liow, X. Tu, G.-Q. Lo, and D.-L. Kwong, "Low-loss high-speed silicon IQ modulator for QPSK/DQPSK in C and L bands," Opt. Express **22**(9), 10703–10709 (2014).
2. X. Zhang, A. Hosseini, X. Lin, H. Subbaraman, and R. T. Chen, "Polymer-based hybrid-integrated photonic devices for silicon on-chip modulation and board-level optical interconnects," IEEE J. Sel. Top. Quantum Electron. **19**(6), 196–210 (2013).
3. R. S. Jacobsen, K. N. Andersen, P. I. Borel, J. Fage-Pedersen, L. H. Frandsen, O. Hansen, M. Kristensen, A. V. Lavrinenko, G. Moulin, H. Ou, C. Peucheret, B. Zsigri, and A. Bjarklev, "Strained silicon as a new electro-optic material," Nature **441**(7090), 199–202 (2006).
4. B. Chmielak, M. Waldow, C. Matheisen, C. Ripperda, J. Bolten, T. Wahlbrink, M. Nagel, F. Merget, and H. Kurz, "Pockels effect based fully integrated, strained silicon electro-optic modulator," Opt. Express **19**(18), 17212–17219 (2011).
5. G. T. Reed, G. Mashanovich, F. Y. Gardes, and D. J. Thomson, "Silicon optical modulators," Nat. Photonics **4**(8), 518–526 (2010).
6. J. Fujikata, J. Ushida, T. Nakamura, Y. Ming-Bin, Z. Shi Yang, D. Liang, P. L. Guo-Qiang, and D. L. Kwong, "25 GHz operation of silicon optical modulator with projection MOS structure," in *Optical Fiber Communication Conference, 2010* (OSA, 2010), p. OMI3.
7. T. Baba, S. Akiyama, M. Imai, T. Akagawa, M. Takahashi, N. Hirayama, H. Takahashi, Y. Noguchi, H. Okayama, T. Horikawa, and T. Usuki, "25-Gbps operation of silicon p-i-n Mach-Zehnder optical modulator with 100-μm-long phase shifter," in *CLEO: Science and Innovations, 2012* (OSA, 2012), p. CF2L.3.
8. P. Dong, X. Liu, S. Chandrasekhar, L. L. Buhl, R. Aroca, and Y.-K. Chen, "Monolithic silicon photonic integrated circuits for compact 100+ Gb/s coherent optical receivers and transmitters," IEEE J. Sel. Top. Quantum Electron. **20**, 1–8 (2014).
9. B. Milivojevic, C. Raabe, A. Shastri, M. Webster, P. Metz, S. Sunder, B. Chattin, S. Wiese, B. Dama, and K. Shastri, "112Gb/s DP-QPSK transmission over 2427km SSMF using small-size silicon photonic IQ modulator and low-power CMOS driver," in *Optical Fiber Communication Conference, 2013* (OSA, 2013), p. OTh1D.1.

#223328 - $15.00 USD Received 23 Sep 2014; revised 3 Nov 2014; accepted 8 Nov 2014; published 21 Nov 2014

10. R. Soref and B. Bennett, "Electrooptical effects in silicon," IEEE J. Quantum Electron. **23**(1), 123–129 (1987).
11. T. Baehr-Jones, M. Hochberg, G. Wang, R. Lawson, Y. Liao, P. A. Sullivan, L. Dalton, A. K.-Y. Jen, and A. Scherer, "Optical modulation and detection in slotted Silicon waveguides," Opt. Express **13**(14), 5216–5226 (2005).
12. C. Koos, J. Brosi, M. Waldow, W. Freude, and J. Leuthold, "Silicon-on-insulator modulators for next-generation 100 Gbit/s-ethernet," in *33rd European Conference and Exhibition of Optical Communication (ECOC)* (VDE, 2007).
13. J. Leuthold, C. Koos, W. Freude, L. Alloatti, R. Palmer, D. Korn, J. Pfeifle, M. Lauermann, R. Dinu, S. Wehrli, M. Jazbinsek, P. Gunter, M. Waldow, T. Wahlbrink, J. Bolten, H. Kurz, M. Fournier, J.-M. Fedeli, H. Yu, and W. Bogaerts, "Silicon-organic hybrid electro-optical devices," IEEE J. Sel. Top. Quantum Electron. **19**(6), 114–126 (2013).
14. J.-M. Brosi, C. Koos, L. C. Andreani, M. Waldow, J. Leuthold, and W. Freude, "High-speed low-voltage electro-optic modulator with a polymer-infiltrated silicon photonic crystal waveguide," Opt. Express **16**(6), 4177–4191 (2008).
15. J. H. Wülbern, S. Prorok, J. Hampe, A. Petrov, M. Eich, J. Luo, A. K.-Y. Jen, M. Jenett, and A. Jacob, "40 GHz electro-optic modulation in hybrid silicon-organic slotted photonic crystal waveguides," Opt. Lett. **35**(16), 2753–2755 (2010).
16. X. Zhang, H. Subbaraman, A. Hosseini, and R. T. Chen, "Highly efficient mode converter for coupling light into wide slot photonic crystal waveguide," Opt. Express **22**(17), 20678–20690 (2014).
17. X. Zhang, A. Hosseini, S. Chakravarty, J. Luo, A. K.-Y. Jen, and R. T. Chen, "Wide optical spectrum range, subvolt, compact modulator based on an electro-optic polymer refilled silicon slot photonic crystal waveguide," Opt. Lett. **38**(22), 4931–4934 (2013).
18. R. Palmer, S. Koeber, W. Heni, D. L. Elder, D. Korn, H. Yu, L. Alloatti, S. Koenig, P. C. Schindler, W. Bogaerts, M. Pantouvaki, G. Lepage, P. Verheyen, J. Van Campenhout, P. Absil, R. Baets, L. R. Dalton, W. Freude, J. Leuthold, and C. Koos, "High-Speed Silicon-Organic Hybrid (SOH) Modulator with 1.6 fJ/bit and 180 pm/V In-Device Nonlinearity," in *39th European Conference and Exhibition on Optical Communication (ECOC 2013)* (IET, 2013).
19. S. Koeber, R. Palmer, M. Lauermann, W. Heni, D. L. Elder, D. Korn, M. Woessner, L. Alloatti, S. Koenig, P. C. Schindler, H. Yu, W. Bogaerts, L. R. Dalton, W. Freude, J. Leuthold, and C. Koos, "Femtojoule electro-optic modulation using a silicon-organic hybrid device," Light Sci. Appl. (to be published).
20. D. Korn, R. Palmer, H. Yu, P. C. Schindler, L. Alloatti, M. Baier, R. Schmogrow, W. Bogaerts, S. K. Selvaraja, G. Lepage, M. Pantouvaki, J. M. D. Wouters, P. Verheyen, J. Van Campenhout, B. Chen, R. Baets, P. Absil, R. Dinu, C. Koos, W. Freude, and J. Leuthold, "Silicon-organic hybrid (SOH) IQ modulator using the linear electro-optic effect for transmitting 16QAM at 112 Gbit/s," Opt. Express **21**(11), 13219–13227 (2013).
21. Y. V. Pereverzev, K. N. Gunnerson, O. V. Prezhdo, P. A. Sullivan, Y. Liao, B. C. Olbricht, A. J. P. Akelaitis, A. K.-Y. Jen, and L. R. Dalton, "Guest–host cooperativity in organic materials greatly enhances the nonlinear optical response," J. Phys. Chem. C **112**(11), 4355–4363 (2008).
22. R. Palmer, S. Koeber, D. Elder, M. Woessner, W. Heni, D. Korn, M. Lauermann, W. Bogaerts, L. Dalton, W. Freude, J. Leuthold, and C. Koos, "High-speed, low drive-voltage silicon-organic hybrid modulator based on a binary-chromophore electro-optic material," J. Lightwave Technol. **32**(16), 2726–2734 (2014).
23. M. Lauermann, R. Palmer, S. Koeber, P. C. Schindler, D. Korn, T. Wahlbrink, J. Bolten, M. Waldow, D. L. Elder, L. R. Dalton, J. Leuthold, W. Freude, and C. G. Koos, "16QAM silicon-organic hybrid (SOH) modulator operating with 0.6 V_{pp} and 19 fJ/bit at 112 Gbit/s," in *CLEO: Science and Innovations* (OSA, 2014), p. SM2G.6.
24. L. Alloatti, D. Korn, R. Palmer, D. Hillerkuss, J. Li, A. Barklund, R. Dinu, J. Wieland, M. Fournier, J. Fedeli, H. Yu, W. Bogaerts, P. Dumon, R. Baets, C. Koos, W. Freude, and J. Leuthold, "42.7 Gbit/s electro-optic modulator in silicon technology," Opt. Express **19**(12), 11841–11851 (2011).
25. L. Alloatti, M. Lauermann, C. Sürgers, C. Koos, W. Freude, and J. Leuthold, "Optical absorption in silicon layers in the presence of charge inversion/accumulation or ion implantation," Appl. Phys. Lett. **103**(5), 051104 (2013).
26. J. Witzens, T. Baehr-Jones, and M. Hochberg, "Design of transmission line driven slot waveguide Mach-Zehnder interferometers and application to analog optical links," Opt. Express **18**(16), 16902–16928 (2010).
27. Y. Enami, J. Luo, and A. K.-Y. Jen, "Short hybrid polymer/sol-gel silica waveguide switches with high in-device electro-optic coefficient based on photostable chromophore," AIP Adv. **1**(4), 042137 (2011).
28. J. Luo, S. Huang, Z. Shi, B. M. Polishak, X.-H. Zhou, and A. K. Jen, "Tailored organic electro-optic materials and their hybrid systems for device applications," Chem. Mater. **23**(3), 544–553 (2011).
29. Z. Shi, W. Liang, J. Luo, S. Huang, B. M. Polishak, X. Li, T. R. Younkin, B. A. Block, and A. K.-Y. Jen, "Tuning the kinetics and energetics of Diels–Alder cycloaddition reactions to improve poling efficiency and thermal stability of high-temperature cross-linked electro-optic polymers," Chem. Mater. **22**(19), 5601–5608 (2010).
30. R. Schmogrow, D. Hillerkuss, M. Dreschmann, M. Huebner, M. Winter, J. Meyer, B. Nebendahl, C. Koos, J. Becker, W. Freude, and J. Leuthold, "Real-time software-defined multiformat transmitter generating 64QAM at 28 GBd," IEEE Photon. Technol. Lett. **22**(21), 1601–1603 (2010).
31. R. Palmer, L. Alloatti, D. Korn, W. Heni, P. C. Schindler, J. Bolten, M. Karl, M. Waldow, T. Wahlbrink, W. Freude, C. Koos, and J. Leuthold, "Low-loss silicon strip-to-slot mode converters," IEEE Photon. J. **5**(1), 2200409 (2013).
32. F. Derr, "Coherent optical QPSK intradyne system: concept and digital receiver realization," J. Lightwave Technol. **10**(9), 1290–1296 (1992).

#223328 - $15.00 USD Received 23 Sep 2014; revised 3 Nov 2014; accepted 8 Nov 2014; published 21 Nov 2014

33. R. Ding, T. Baehr-Jones, W.-J. Kim, B. Boyko, R. Bojko, A. Spott, A. Pomerene, C. Hill, W. Reinhardt, and M. Hochberg, "Low-loss asymmetric strip-loaded slot waveguides in silicon-on-insulator," Appl. Phys. Lett. **98**(23), 233303 (2011).
34. D. Vermeulen, S. Selvaraja, P. Verheyen, G. Lepage, W. Bogaerts, P. Absil, D. Van Thourhout, and G. Roelkens, "High-efficiency fiber-to-chip grating couplers realized using an advanced CMOS-compatible silicon-on-insulator platform," Opt. Express **18**(17), 18278–18283 (2010).
35. N. Lindenmann, S. Dottermusch, T. Hoose, M. R. Billah, S. Koeber, W. Freude, and C. Koos, "Connecting silicon photonic circuits to multi-core fibers by photonic wire bonding," in *Optical Interconnects Conference, 2014* (IEEE, 2014), pp. 131–132.
36. N. Lindenmann, S. Dottermusch, M. L. Goedecke, T. Hoose, M. R. Billah, T. Onanuga, A. Hofmann, W. Freude, and C. Koos, "Connecting silicon photonic circuits to multi-core fibers by photonic wire bonding," J. Lightwave Technol. (to be published).
37. R. Schmogrow, B. Nebendahl, M. Winter, A. Josten, D. Hillerkuss, S. Koenig, J. Meyer, M. Dreschmann, M. Huebner, C. Koos, J. Becker, W. Freude, and J. Leuthold, "Error vector magnitude as a performance measure for advanced modulation formats," IEEE Photon. Technol. Lett. **24**, 61-63 (2012). Correction: ibid., 24, 2198 (2012)
38. R.-J. Essiambre, G. Kramer, P. J. Winzer, G. J. Foschini, and B. Goebel, "Capacity limits of optical fiber networks," J. Lightwave Technol. **28**(4), 662–701 (2010).

1. Introduction

Electro-optical in-phase and quadrature (IQ) modulators are key elements for spectrally efficient coherent transmission in high-speed telecommunication links [1] and optical interconnects [2]. As key requirements, the devices must combine small footprint and high electro-optic bandwidth with low drive voltages and therefore low power consumption. In principle, silicon photonics is a particularly promising platform for realizing such devices, offering high-density photonic-electronic integration at low cost by exploiting large-scale high-yield complementary metal-oxide-semiconductor (CMOS) processing. However, bulk silicon does not feature any second-order optical nonlinearities due to the inversion symmetry of the crystal lattice. Strain can be used to break the crystal symmetry of silicon and to allow for nonzero $\chi^{(2)}$-coefficients [3] which have been exploited to realize Mach-Zehnder modulators [4], but the reported modulation efficiencies are still comparatively low. As a consequence, current silicon-based modulators have to rely on free-carrier depletion or injection in p-n, p-i-n, or in metal-oxide-semiconductor (MOS) structures [5–7]. This leads to various trade-offs, particularly when realizing fast and energy-efficient IQ modulators. An all-silicon dual-polarization 16QAM modulator was demonstrated recently [8] using conventional depletion-type p-n-phase shifters. Operating the device with a peak-to-peak drive voltage of 5 V_{pp} at a symbol rate of 28 GBd, an energy consumption of 1.2 pJ/bit and bit error ratios (BER) between 1×10^{-2} and 2.4×10^{-2} have been achieved. These are remarkable results, but the potential for further optimization towards lower drive voltages, reduced energy consumption and smaller footprint seems to be limited by the intrinsically rather low modulation efficiency of depletion-type phase shifters — the voltage-length product of the device [8] amounts to $U_\pi L$ = 24 Vmm. Drive voltages can be reduced at the expense of an increased drive current by replacing the pn-junction with a high-capacitance metal-oxide-semiconductor structure [9]. Such devices require drive voltages of only 1 V_{pp}, but have hitherto been demonstrated for QPSK modulation only. Moreover, both injection and depletion-type modulators suffer from amplitude-phase coupling: Phase modulation in these devices is based on free carriers, the presence of which does not only lead to a change of the refractive index, but also to free-carrier absorption [10]. The associated amplitude modulation may lead to signal distortions when using higher-order modulation formats such as 16QAM, where independent information is encoded on amplitude and phase of the optical carrier.

Silicon-organic hybrid (SOH) integration promises to overcome the inherent limitations of free-carrier plasma dispersion as a modulation mechanism by combining silicon-on-insulator (SOI) slot waveguides with organic electro-optic (EO) claddings [11–13]. These slot waveguides can be integrated in photonic-crystal structures that allow reduction of the optical group velocity and hence intensify the interaction of the optical mode with the EO material [14–16]. Voltage-length products of $U_\pi L$ = 0.29 Vmm were demonstrated by exploiting slow light [17], but practical applications have to cope with the limited bandwidth ranges over which the group delay is flat and dispersion is small, and with the resulting need for

#223328 - $15.00 USD Received 23 Sep 2014; revised 3 Nov 2014; accepted 8 Nov 2014; published 21 Nov 2014

wavelength tuning. Non-resonant SOH Mach-Zehnder modulators are more versatile, and modulation experiments with on-off-keying at data rates of 12.5 Gbit/s demonstrated an ultra-low energy consumption of 1.6 fJ/bit [18,19]. At these low data rates the modulator could be driven without termination resistor. However, when using advanced modulation formats two nested Mach-Zehnder modulators are needed, and higher data rates require a termination of the modulator electrodes. As a consequence, the energy consumption increases considerably, e. g., to 640 fJ/bit measured in a 16QAM modulation experiment at a symbol rate of 28 GBd and a BER of 1.2×10^{-3} [20].

In this paper we show that a novel class of organic cladding materials [21,22] can dramatically improve the performance and simultaneously decrease the power consumption of SOH IQ modulators. Using conventional slot waveguides, our devices feature voltage-length products of only $U_\pi L = 0.53$ Vmm — a factor of 20 smaller than that of current all-silicon modulators, and only slightly larger than those of slow-light devices. Operating a 1.5 mm long device at a peak-to-peak drive voltage of only 0.6 V_{pp}, we demonstrate error-free QPSK modulation at a data rate of 56 Gbit/s and 16QAM signaling at 112 Gbit/s with a BER of 5.1×10^{-5} [23]. For the 16QAM experiment, the energy consumption of the modulator is calculated to be only 19 fJ/bit. This is the lowest drive voltage and the lowest energy consumption that have so far been reported for a 28 GBd 16QAM modulator, regardless of the material system. Moreover, the BER of 5.1×10^{-5} corresponds to the lowest value achieved with silicon-based devices for 16QAM at such symbol rates. While this is a first proof-of-concept experiment, we believe that SOH integration has vast potential of further improving the performance of silicon-based IQ modulators, both in terms of symbol rate and modulation efficiency.

2. Silicon-organic hybrid (SOH) modulator

The SOH IQ modulator consists of two nested 1.5 mm long Mach-Zehnder modulators (MZM), each driven by a single coplanar transmission line in ground-signal-ground (GSG) configuration, see Fig. 1(a). The phase modulators of the MZM consist of SOI slot waveguides, which are covered by an EO material. When operating the optical slot waveguide in quasi-TE polarization, enhancement of the electric field in the slot leads to strong interaction of the guided light within the EO cladding, see Fig. 1(c) for a plot of the E_x component of the optical field. At the same time, the slot waveguide is connected to aluminum transmission lines by thin, lightly *n*-doped silicon slabs, which results in a strong RF modulation field between the rails and hence in a large overlap with the optical mode, see Fig. 1(d) [13]. In contrast to conventional silicon modulators based on the plasma dispersion effect, SOH devices do not exhibit amplitude-phase coupling and enable pure phase modulation [24]. The conductivity of the slab is increased by applying a gate voltage U_{gate} between the substrate and the SOI device layer [25], Fig. 1(a).

The devices were fabricated on an SOI wafer with 220 nm-thick SOI device layer and 3 µm-thick buried oxide (BOX), using a combination of electron-beam lithography for structuring the optical waveguides and optical lithography for the metallization. The fabricated slot width is $w_{slot} = 80$ nm, and the rail width amounts to $w_{rail} = 240$ nm. The transmission line consists of 200 nm thick aluminum strips in a ground-signal-ground (GSG) configuration [26]. The parts of the silicon slab which are overlapping with the aluminum are highly *n*-doped to achieve an Ohmic contact. The central conductor of the GSG transmission line has a width of approximately 10 µm, and the signal-ground electrode separation is approximately 5 µm. The transmission line is designed with CST Microwave Studio, the model includes the doping of the silicon slabs by introducing a small conductivity in the material. Electrical characterization of the fabricated device with a 50 Ω probe shows low back reflections of the RF signal with S_{11} magnitudes of less than −20 dB at frequencies of up to 40 GHz and the actual device impedance amounts to 50 ± 5 Ω. The group refractive index mismatch is $n_{opt} - n_{RF} = 0.4$ and thus the walk-off is so small that it does not significantly influence the bandwidth at a device length of 1.5 mm.

#223328 - $15.00 USD Received 23 Sep 2014; revised 3 Nov 2014; accepted 8 Nov 2014; published 21 Nov 2014

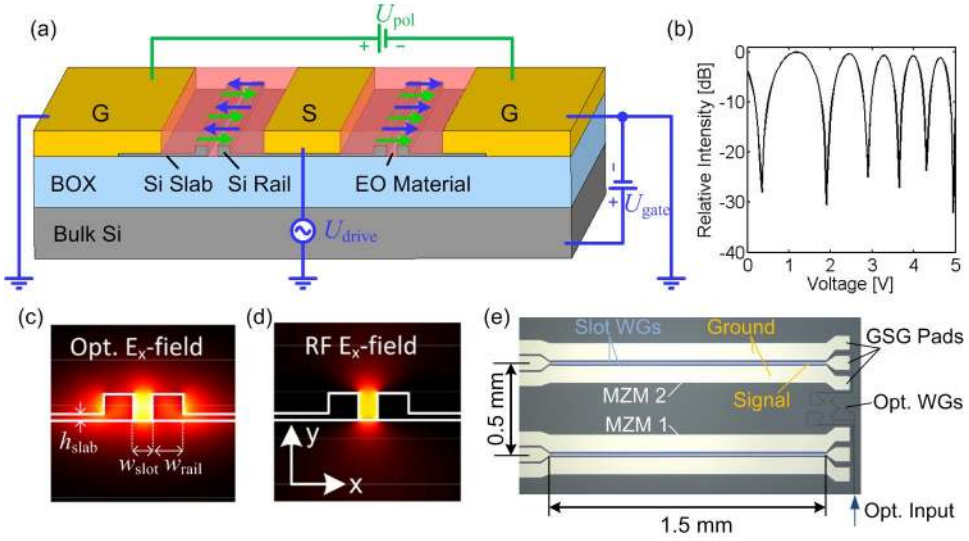

Fig. 1. (a) Cross-section of a silicon-organic hybrid (SOH) Mach-Zehnder modulator (MZM). Each arm contains a slot waveguide (rail width w_{rail} = 240 nm, slot width w_{slot} = 80 nm). The device is coated with an electro-optic (EO) organic cladding material, consisting of a mixture of the EO chromophores YLD124 and PSLD41 [21,22]. The waveguides are electrically connected to a ground-signal-ground (GSG) RF transmission line via *n*-doped silicon slabs (thickness h_{slab} = 70 nm). A gate voltage U_{gate} between the Si substrate and the SOI device layer improves the conductivity of the silicon slab and hence the bandwidth of the device. A poling voltage U_{pol} is initially applied via the floating ground electrodes of the device to align the chromophores in the slots of both waveguides (green arrows). When operating the device via the GSG line, the modulating electric RF field (blue arrows) is anti-parallel (parallel) to the chromophore orientation in the left (right) half of the GSG line. This results in opposite phase shifts in the two arms of the MZM and hence in push-pull operation. (b) Transmission vs. DC voltage of a MZM having 1.5 mm long phase shifters. At bias voltages above 2.9 V, the π-voltage of the device amounts to U_π = 0.35 V. For smaller DC voltages, free charges in the cladding lead to a partial screening of the applied electric field and hence to increased π-voltages. (c) E_x component of the optical field in the slot waveguide. (d) Dominant E_x component of the electrical drive signal. Both fields are confined to the slot, resulting in strong interaction and hence efficient modulation. (e) Optical micrograph of the IQ modulator structure prior to depositing the organic cladding. The GSG transmission lines of both MZM are clearly visible. For contacting, the GSG line is up-tapered at both ends of the slot waveguide section to match the 100 µm pitch of the microwave probe.

For the EO material, we use a mixture of the multi-chromophore dendritic molecule PSLD41 (75 wt.-%) and the chromophore YLD124 (25 wt.-%) [21,22]. This binary-chromophore organic glass (BCOG) has a refractive index of n = 1.73 and shows in bulk material an r_{33} coefficient of 285 pm/V [21]. The in-device material-related r_{33} of 230 pm/V reported in [22] with this BCOG corresponds to the highest value shown so far for SOH devices. The material is deposited via spin coating, and a poling step is performed for aligning the randomly oriented chromophores. To this end, the EO material is heated close to its glass transition temperature of 97 °C while applying a poling voltage across the two floating ground electrodes, see Fig. 1(a). This leads to an ordered orientation of the dipolar chromophores along the poling field, indicated by green arrows in Fig. 1(a). The orientation of the chromophores is frozen by cooling the device back to room temperature before removing the poling voltage. For operating the device, an RF signal is coupled to the GSG transmission line, leading to a modulating electric field as indicated by blue arrows in Fig. 1(a). The RF field and the chromophore orientation are antiparallel to each other in the left half of the GSG transmission line, and parallel in the right half. This leads to phase shifts of opposite signs in the two arms of the MZM as needed for push-pull operation. To establish good electrical

#223328 - $15.00 USD Received 23 Sep 2014; revised 3 Nov 2014; accepted 8 Nov 2014; published 21 Nov 2014

contact for the microwave probes, the EO material is mechanically removed at the contact pads. An intentional imbalance in the parent MZM allows to adjust a π/2 phase shift between the in-phase (I) and quadrature (Q) component via wavelength tuning, see Fig. 2(a). Characterization of one of the MZM at DC voltages exhibits a π-voltage U_π for the push-pull modulator of only 0.35 V for bias voltages of more than 2.9 V, see Fig. 1(b). The phase shifters of the device are 1.5 mm long, resulting in a voltage-length product as low as $U_\pi L$ = 0.53 Vmm for push-pull operation, which enables low-power operation of the IQ modulator. For smaller bias voltages, we observe increased spacings of the transmission dips in Fig. 1(b) and hence increased π-voltages. This is attributed to free charges in the cladding that lead to a partial screening of the applied fields at small bias voltages. Due to the low mobility of the free charges, this is only observable for low frequencies and does not impede high frequency operation. An optical micrograph of the SOH device prior to depositing the organic cladding is shown in Fig. 1(e). From the measured U_π we can calculate the electro-optic coefficient r_{33} with the relation [22,26]

$$r_{33} = \frac{w_{slot}\lambda_c}{2LU_\pi \Gamma n_{slot}^3}, \tag{1}$$

where w_{slot} denotes the slot width, λ_c is the wavelength of the optical carrier, L the modulator length and n_{slot} the refractive index of the organic material in the slot. The field interaction Γ is linked to the fraction of the optical power that interacts with the modulation field [22,26]. Our device geometry is optimized for a maximum field interaction, which amounts to Γ = 0.22. Using Eq. (1) the electro-optic coefficient is determined to be 104 pm/V. The poling efficiency $r_{33}/E_{\mathrm{poling}}$ amounts to 0.28 $\mathrm{nm^2/V^2}$ for this particular device.

For practical applications of SOH devices, the long-term stability of the organic cladding is of high importance. Materials have become available featuring glass transition temperatures of more than 130 °C while maintaining electro-optic coefficients in excess of 100 pm/V [27]. The investigation of aging and temperature stability of organic EO materials is subject to ongoing research. It can be expected that the stability of the materials can be further improved by synthetically modified chromophores that bear specific crosslinking agents for post-poling lattice hardening or by increasing the molar mass of the chromophores. The viability of the first approach has been demonstrated for similar EO compounds [28,29] where material stability of up to 250°C has been achieved.

3. Signal generation experiment

The experimental setup for generation of data signals is depicted in Fig. 2(a). Light from an external-cavity laser is coupled to the chip via grating couplers. The electrical non-return-to-zero (NRZ) drive signals are generated in software-defined multi-format transmitters, based on field-programmable gate arrays (FPGA) [30] and operated at a symbol rate of 28 GBd. The transmitters comprise a pair of digital-to-analog converters (DAC) that are directly coupled to the two on-chip MZM using RF probes, without any additional amplification. The electrical transmission line of each MZM features an impedance close to 50 Ω, matched to the output impedance of the DAC, and is terminated with an external 50 Ω resistor to avoid back reflections at the end of the transmission line.

#223328 - $15.00 USD Received 23 Sep 2014; revised 3 Nov 2014; accepted 8 Nov 2014; published 21 Nov 2014

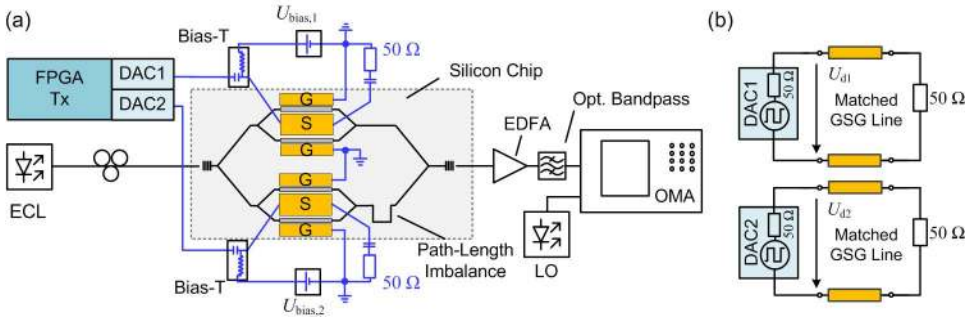

Fig. 2. Schematic of the experimental setup. (a) Two nested MZM form an IQ modulator. An intentional path-length imbalance in the parent Mach-Zehnder interferometer allows for adjusting the phase difference of in-phase (I) and quadrature-phase (Q) component of the signal to $\pi/2$ by wavelength tuning. Electrical multilevel drive signals are generated by field-programmable gate arrays (FPGA) and high-speed digital-to-analog converters (DAC), the outputs of which are directly coupled to the silicon chip via microwave probes. Bias-Ts are used to apply DC bias voltages to the MZM for adjusting the operating points. An external-cavity laser (ECL) is used as an optical source and coupled to the chip via fibers and grating couplers. The optical output signal is amplified by an EDFA and subsequently fed into an optical modulation analyzer (OMA) with a second laser as local oscillator (LO). (b) Equivalent-circuit diagram of the experimental setup for calculation of the energy consumption. Each MZM features a 50 Ω GSG transmission line which is terminated by an external 50 Ω resistor and is driven directly by one DAC, represented by an ideal voltage source and an internal resistance of 50 Ω. The GSG line of the MZM is matched to the 50 Ω output of the DAC. To estimate the energy consumption, we can replace the transmission line and its termination by an equivalent resistor of R = 50 Ω.

A gate field of E_{gate} = 0.1 V/nm is applied between the silicon substrate and the SOI device layer to increase the bandwidth [25]. To apply the gate voltage, the SOH chip is placed on an electrically isolated sample mount which can be set to a defined potential with respect to the ground of the microwave probes. To avoid high gate voltages across the 3 µm BOX in the future, we plan to deposit a silicon layer on top of the silicon slabs, isolated from the slabs by a thin silicon oxide film [24]. This structure features a thin gate oxide with only a few nanometers thickness and can thereby reduce the necessary gate voltage to a few volts only. Negligible current flow is associated with the applied gate voltage, and the energy consumption of the device is hence not increased. The fiber-to-fiber insertion loss of the silicon chip, obtained from a transmission measurement without modulation signal or gate voltage and with the modulator tuned to maximum transmission, amounts to 27 dB. It is compensated by an erbium-doped fiber amplifier (EDFA). The rather high optical insertion loss of our modulator originates mainly from the losses of the non-optimized grating couplers (together 10 dB), the losses of the 9 mm long access strip waveguides (0.5 dB/mm due to sidewall roughness), from the losses of the optimized strip-to-slot converters [31] and multimode interference couplers (MMI) (together 1 dB), and from the propagation loss in the 1.5 mm long slot waveguide section of the phase shifter (approx. 6.5 dB/mm caused by roughness and below 1 dB/mm by doping [10]). A bandpass-filter is inserted after the EDFA to remove out-of-band amplified spontaneous emission (ASE) noise from the EDFA. The signal is then detected by an optical modulation analyzer (OMA), using a second external-cavity laser as a local oscillator (LO) in an intradyne configuration [32]. Standard digital post-processing comprising polarization demultiplexing, compensation of the frequency offset between the transmitter laser and the LO, phase recovery and channel equalization is applied at the OMA. The optical insertion loss of the current modulator is still rather high, but we expect that losses can be reduced considerably in future device generations. As an example, the insertion loss of undoped slot waveguides can be decreased well below 1 dB/mm by using asymmetric waveguide geometries and by improving the sidewall roughness [33]. Moreover, optimization of doping profiles outside the region where the light is guided might allow to operate the device without a gate field which causes 1 dB – 2 dB optical loss, and to decrease

#223328 - $15.00 USD Received 23 Sep 2014; revised 3 Nov 2014; accepted 8 Nov 2014; published 21 Nov 2014

the total carrier-induced propagation loss that currently amounts to approx. 3 dB/mm. Similarly, using optimized grating couplers [34] or photonic wire bonds [35,36], the coupling loss to external fibers can be improved to below 2 dB per chip facet.

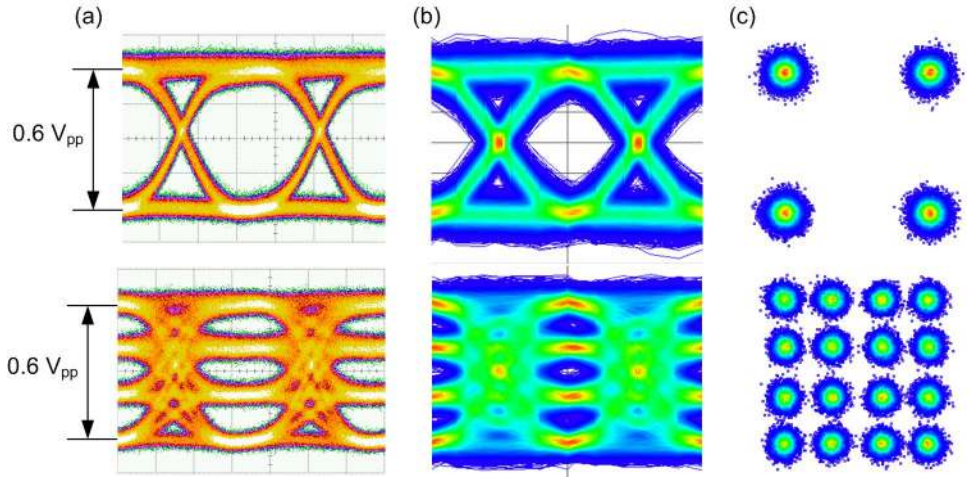

Fig. 3. Measured eye diagrams and constellations for a symbol rate of 28 GBd. (a) Eye diagram of the electrical drive signals for one MZM in the case of QPSK (top) and 16QAM (bottom). Peak-to-peak drive voltages of 0.6 V_{pp} are sufficient to generate a high-quality optical signal. The eye diagrams were obtained by connecting an oscilloscope with a 50 Ω input impedance to the DAC that are used to drive the modulators. (b) Corresponding optical eye diagrams, measured with the optical modulation analyzer. (c) Corresponding constellation diagrams of the optical signals. The measured EVM_m of the QPSK signal is 10.9%; no errors could be measured. From the measured EVM_m, the BER can be estimated to be well below to 1×10^{-10}. For the 16QAM signal, the EVM_m is 8.7% and the measured BER amounts to 5.1×10^{-5}.

In a first modulation experiment, a QPSK signal at 28 GBd is generated, derived from a pseudorandom binary sequence (PRBS) with a length of $2^{11} - 1$. The electrical eye diagram of one channel is depicted in Fig. 3(a). The eye diagram was obtained by connecting an oscilloscope with 50 Ω input impedance to the output of the DAC, and the measured voltage levels are hence identical to the drive voltages of the 50 Ω MZM. The peak-to-peak voltages of the electrical drive signals are found to be 0.60 V for the I-channel and 0.63 V for the Q-channel. The voltages are measured at the end of the RF cable, before connecting to the microwave probes. The measured optical eye diagram of one channel and the constellation diagram are depicted in Fig. 3(b) and 3(c), top row. As a quantitative measure of the signal quality, we use the error vector magnitude (EVM_m), which describes the effective distance of a received complex symbol from its ideal position in the constellation diagram, using the maximum length of an ideal constellation vector for normalization. For the QPSK signal, the EVM_m is measured to be 10.9%. If we assume additive white Gaussian (AWGN) noise as main limitation of our received signal, we can relate this EVM_m to a bit error ratio (BER) well below 1×10^{-10} [37]. Within the recorded 62.5 µs signal section, we measure 1.7×10^6 symbols, so a direct measurement of a BER was not possible.

In a second experiment, a 16QAM signal is generated [23]. The electrical 4-level signal of the I-channel is shown in Fig. 3(a), along with the optical eye diagram and the corresponding constellation diagram measured at 28 GBd, Fig. 3(b) and (c), bottom row. The measured BER is 5.1×10^{-5} and the EVM_m of the signal is 8.7%. This EVM_m would correspond to a calculated BER of 4.8×10^{-5}, which is in very good agreement with the measured value. The good match between the calculated and measured BER supports the assumption that the signal quality is limited by AWGN only. The signal to noise ratio (SNR) is measured at the OMA after coherent reception and amounts to 20.4 dB within the evaluated signal bandwidth of 40 GHz. This corresponds to an optical SNR (OSNR) of 22.4 dB at a reference bandwidth of

#223328 - $15.00 USD Received 23 Sep 2014; revised 3 Nov 2014; accepted 8 Nov 2014; published 21 Nov 2014

0.1 nm with noise in both polarizations [38]. Furthermore, we see in Fig. 3(c) very regular constellation diagrams without distortion or rotation, from which we can conclude that the SOH modulator provides indeed pure phase modulation without any residual amplitude-phase coupling. For high-speed operation, the π-voltage increases due to bandwidth limitations [26]. A characterization of one MZM results in a 6 dB electro-optic-electric (3 dB electro-optic) bandwidth of 18 GHz and U_π at symbol rates of 28 GBd can be estimated to 0.7 V, resulting in a corresponding voltage-length product of $U_\pi L$ = 1.05 Vmm and a modulation index of U/U_π = 0.86.

4. Energy consumption

For estimating the energy consumption of our devices, we use an equivalent circuit of the MZM and the driver electronics, see Fig. 2(b): Each DAC, represented by an ideal voltage source and an internal resistance of 50 Ω, is connected to a 50 Ω transmission line that represents the MZM and that is terminated by a matched 50 Ω resistor. For estimating the power consumption of the MZM, we can replace the transmission line and its termination by an equivalent resistor of R = 50 Ω. The power consumption of a single MZM is then given by the power dissipation in this resistor, and the energy per bit for the IQ modulator is obtained by adding the power consumptions of the two MZM and dividing by the total data rate. For QPSK, assuming rectangular non-return-to-zero drive signals and equal probability of all symbol states, the energy consumption per bit for the IQ modulator can be calculated according to

$$W_{\mathrm{bit,QPSK}} = \left[\left(\frac{U_{\mathrm{d1}}}{2}\right)^2 \frac{1}{R} + \left(\frac{U_{\mathrm{d2}}}{2}\right)^2 \frac{1}{R}\right] \times \frac{1}{r_{\mathrm{QPSK}}}. \tag{2}$$

The quantities $U_{\mathrm{d1,2}}$ are the peak-to-peak voltages of the electrical drive signals, measured across the equivalent resistor of R = 50 Ω, which amount to 0.60 V for the I and 0.63 V for the Q-channel. The aggregate data rate is r_{QPSK} = 56 Gbit/s for the QPSK signal, leading to a power consumption of 68 fJ/bit.

For 16QAM, the energy consumption per bit can be calculated similarly. For each MZM, the power of the drive signal is dissipated in the equivalent 50 Ω-resistor. However, the drive signal of each MZM now consists of two amplitude levels, which differ by a factor of 1/3. Assuming again equal distribution of the various symbols, the energy of each MZM can be calculated by averaging over the dissipated energy of both amplitude levels. The energy per bit is then obtained by adding the power consumption of the two MZM and dividing by the total data rate,

$$W_{\mathrm{bit,16QAM}} = \left(\frac{1}{2}\left[\left(\frac{U_{\mathrm{d1}}}{2}\right)^2 \frac{1}{R} + \left(\frac{1}{3}\frac{U_{\mathrm{d1}}}{2}\right)^2 \frac{1}{R}\right] + \frac{1}{2}\left[\left(\frac{U_{\mathrm{d2}}}{2}\right)^2 \frac{1}{R} + \left(\frac{1}{3}\frac{U_{\mathrm{d2}}}{2}\right)^2 \frac{1}{R}\right]\right) \times \frac{1}{r_{\mathrm{16QAM}}}. \tag{3}$$

Using the measured peak-to-peak voltages of U_{d1} = 0.60 V and U_{d2} = 0.63 V and a data rate of r_{16QAM} = 112 Gbit/s, the energy consumption of the modulator is found to be 19 fJ/bit for the case of 16QAM signaling. This is, to the best of our knowledge, the lowest energy consumption that has so far been reported for a 16QAM modulator at such symbol rates, regardless of the material system. Applying DC bias and gate voltages to the modulator leads to a very small current flow around 1 nA. The corresponding energy consumption amounts to few aJ/bit and can safely be neglected. It should be noted that the power consumption has been estimated for a modulator with an ideal impedance of 50 Ω. Input impedances deviating from this value would lead to non-perfect impedance matching in our experiment and hence to partial reflection of the RF drive signal. As a consequence, the power consumption of the real device should then even be slightly smaller than the values estimated above, and our estimation of the power consumption hence represents a worst-case scenario.

#223328 - $15.00 USD Received 23 Sep 2014; revised 3 Nov 2014; accepted 8 Nov 2014; published 21 Nov 2014

5. Summary

We experimentally show that the combination of novel EO materials and slot waveguide structures enables silicon-based IQ modulators with unprecedented performance. We demonstrate generation of 28 GBd QPSK and 16QAM signals, leading to data rates of 56 Gbit/s, and 112 Gbit/s, respectively. Using record-low peak-to-peak drive voltages of U_d = 0.6 V, we obtain error-free QPSK modulation and 16QAM signals with a BER of 5.1×10^{-5}. The drive signal is derived directly from the output of the DAC, without the need for an additional driver amplifier. For the 16QAM experiment, we estimate an energy consumption of only 19 fJ/bit — the lowest value reported so far for 16QAM signaling at 28 GBd.

Acknowledgments

We acknowledge support by the European Research Council (ERC Starting Grant 'EnTeraPIC', number 280145), the EU-FP7 projects PhoxTroT and BigPipes, the Alfried Krupp von Bohlen und Halbach Foundation, the Karlsruhe International Research School for Teratronics (HIRST), the Karlsruhe School of Optics and Photonics (KSOP), the DFG Center for Functional Nanostructures (CFN), the Karlsruhe Nano-Micro Facility (KNMF), the Initiative and Networking Fund of the Helmholtz Association, the Deutsche Forschungsgemeinschaft, and the Open Access Publishing Fund of Karlsruhe Institute of Technology. We further acknowledge financial support of the National Science Foundation (DMR-0905686, DMR-0120967, DMR-1303080) and the Air Force Office of Scientific Research (FA9550-09-1-0682).